Creating a capture zone in microfluidic flow greatly enhances the throughput and efficiency of cancer detection

Mingrui Sun[1#], Jiangsheng Xu[1,2,3#], James G. Shamul[2], Xiongbin Lu[4], Syed Husain[3,5] & Xiaoming He[1,2,3,6,7]*

[1]Department of Biomedical Engineering, The Ohio State University, Columbus, OH 43210, USA

[2]Fischell Department of Bioengineering, University of Maryland, College Park, MD 20742, USA

[3]Comprehensive Cancer Center, The Ohio State University, Columbus, Ohio 43210, USA

[4]Department of Medical and Molecular Genetics, Indiana University School of Medicine, Indianapolis, Indiana 46202, USA

[5]Department of Surgery, The Ohio State University Medical Center, Columbus, OH 43210, USA

[6]Robert E. Fischell Institute for Biomedical Devices, University of Maryland, College Park, MD 20742, USA

[7]Marlene and Stewart Greenebaum Comprehensive Cancer Center, University of Maryland, Baltimore, MD 21201, USA

*Corresponding author

Email address: shawnhe@umd.edu

#Contributed equally

Supplementary Data Available (Figs. S1-S13, Movies S1-S6, and Tables S1-S2)

This is the author's manuscript of the article published in final edited form as:

Sun, M., Xu, J., Shamul, J. G., Lu, X., Husain, S., & He, X. (2019). Creating a capture zone in microfluidic flow greatly enhances the throughput and efficiency of cancer detection. Biomaterials. https://doi.org/10.1016/j.biomaterials.2019.01.014

Abstract

Efficient capture of rare circulating tumor cells (CTCs) from blood samples is valuable for early cancer detection to improve the management of cancer. In this work, we developed a highly efficient microfluidics-based method for detecting CTCs in human blood. This is achieved by creating separate capture and flow zones in the microfluidic device (ZonesChip) and using patterned dielectrophoretic force to direct cells from the flow zone into the capture zone. This separation of the capture and flow zones minimizes the negative impact of high flow speed (and thus high throughput) and force in the flow zone on the capture efficiency, overcoming a major bottleneck of contemporary microfluidic approaches using overlapping flow and capture zones for CTC detection. When the flow speed is high (≥ 0.58 mm/s) in the flow zone, the separation of capture and flow zones in our ZonesChip could improve the capture efficiency from ~0% (for conventional device without separating the two zones) to ~100%. Our ZonesChip shows great promise as an effective platform for the detection of CTCs in blood from patients with early/localized-stage colorectal tumors.

Keywords: capture zone; flow zone; microfluidics; CTCs; dielectrophesis; detection

1. Introduction

Cancer is a major public health problem worldwide and is the second leading cause of death in the United States. In 2018, 1,735,350 new cancer cases and 609,640 cancer deaths are estimated by the American Cancer Society [1]. Colorectal cancer (CRC) is the third most commonly diagnosed cancer among both men and women in the United States, and the second- and third-leading cause of cancer-related deaths for men and women, respectively. Patients diagnosed with localized-stage CRC have a 5-year survival rate of 90%, while the survival rate dramatically declines to 14% for patients diagnosed with advanced-stage CRC [2,3]. Cancer progression ends in metastasis in critical organ such as the lungs, liver, bone and brain, which is the major cause of cancer death [4]. Therefore, early detection of the disease may result in the disparities in cancer survival if timely treatment is conducted. One of the major steps that cancer cells undertake to establish the metastatic tumor is that the primary cancer cells invade the surrounding parenchyma and intravasate into blood to circulate and spread [5]. These rare circulating tumor cells (CTCs) are considered to be a valuable target for early detection and characterization of cancers [6-16]. Due to their extremely low concentration in human blood, especially for early localized-stage patients, detection of hundreds (or less) of CTCs from more than one billion blood cells (per milliliter) has been challenging and methods for effective and high-throughput capture of the CTCs are in need. Recently, microfluidics has been explored as a promising platform for sensitive detection of CTCs. For example, microfluidics-based methods have been developed to capture/enrich CTCs from blood samples by modifying the surface of microfluidic channels with antibodies/ligands that specifically bind to CTCs [17-21], and by utilizing the differences in size or/and physical properties between CTCs and white blood cells (WBCs) [22-31]. A major advantage of the size or/and physical property-based methods is that they are label-free and continuous. However, this method may be limited by the fact that the size and physical properties of both CTCs and WBCs are not homogeneous, and there may be significant overlap between CTCs and WBCs in terms of both size and physical properties.

Antibody-based approaches have been widely studied to specifically capture CTCs from human blood [17-19]. The effectiveness of these approaches may be further enhanced by using additional

designs/features such as microvortex-generating herringbone [18], and anti-EpCAM antibody-functionalized graphene oxide nanosheets [19]. However, the antibody-based methods reported so far do not differentiate the capture versus flow zones, which is a bottleneck that limits the throughput of the methods. This is because a high flow speed (and thus high flow-induced force) reduces the possibility of contact between CTCs and the antibody modified on the channel surface, and increases the possibility of the captured CTCs being washed away by the high flow-induced force.

To resolve the aforementioned bottleneck, we developed a microfluidic device with separate capture and flow zones (ZonesChip) for highly efficient antibody-based capture of CTCs from human blood. The cells are moved from the flow zone into the capture zone by applying an external force (dielectropheresis or DEP force in this study). The flow speed in the capture zone is low, which not only facilitates the binding between CTCs and antibody on the microposts, but also reduces the possibility of the captured cells being washed away by the flow-induced force. Our results indicate that at high flow speed (≥ 0.58 mm/s), this separation of the flow and capture zones can improve the efficiency of capturing spiked cancer cells to ~100% from <1.5% for conventional devices with overlapping flow and capture zones. In these conventional devices, the injected cells stay dominantly in the flow zone, limiting their likelihood of being captured. Moreover, our approach is demonstrated to work efficiently for detecting CTCs in human blood samples from CRC patients at an early/localized stage.

2. Materials and methods

2.1. Materials

PC-3 human prostate cancer cells, HCT-116 human colon carcinoma cells, SK-MES-1 human lung cancer cells, OVCAR-3 human ovarian carcinoma cells, MCF-7 human breast cancer cells, and CAPAN-2 human pancreatic adenocarcinoma cells were purchased from American Type Culture Collection (ATCC, Manassas, VA, USA). RBC lysis buffer, neutravidin, biotinylated EpCAM antibody, and N-ymaleimidobutyryloxy succinimide ester (GMBS) were purchased from ThermoFisher Scientific (Waltham, MA, USA). All other materials were purchased from Sigma (St.

Louis, MO, USA) if the source of materials was not specifically mentioned.

2.2. Experimental setup

As show in Fig. 1a and Fig. S1, inlet 1 was connected to a syringe filled with DEP buffer consisting of 10% (w/v) sucrose and 0.3% (w/v) glucose in deionized water. The DEP buffer was introduced into the device via inlet 2 to remove air and fill the channel in the device before the capture experiments. Cells suspended in the DEP buffer were introduced into the device via inlet 2 and collected from the outlet. Microposts were fabricated and patterned in the main channel as that shown in Fig. 1a. The diameter of the microposts was 100 μm, and the gap between two adjacent microposts was 50 μm. The height of the channel was 100 μm. Electrodes 1 and 2, made of copper (Pololu, Las Vegas, NV United States), were inserted into the space between the sidewall and the microposts immediately next to the sidewall in the main channel on both sides of the device, for applying the patterned electric voltage on the device. The microcontroller was programmed to turn the switch on (for 3 s) and off (for 3, 3, 1, 0.5, 0.25 s when the flow rate was 0.1, 0.5, 1, 2, and 4 mL/hr, respectively). The times for on and off are determined based on preliminary experiments, to make sure that there was enough time to drive cells from the flow zone into the capture zone to contact with the surface of the microposts when the DEP was on, and there was sufficient time to drive the non-captured cells back to the flow zone from the capture zone when the DEP was off.

2.3. Fabrication of microfluidic device

Photoresist SU-8 2025 (MicroChem, Westborough, MA, USA) was spin-coated on the surface of a 4-inch silicon wafer with a thickness of 100 μm. The photoresist was soft baked, exposed through patterned mask, post baked, developed using the SU-8 developer (MicroChem, Westborough, MA, USA), and hard baked to obtain photoresist mold. PDMS (Dow Corning, Midland, MI, United States) pre-polymer and its crosslinking agent were mixed thoroughly at a mass ratio of 10:1, poured over the photoresist mold, and cured at 72 °C for 3 h. Afterwards, the crosslinked PDMS layer with patterned structures was peeled off from the photoresist mold. Finally, the PDMS layer and a glass slide were treated by oxygen plasma and then bonded together followed by surface modification with antibody.

2.4. Surface modification with antibody

The surface was modified according to a previously reported method with slight modification.[17] Briefly, after bonding the PDMS and glass slide, the device was filled with 4% (v/v) 3-mercaptopropyl trimethoxysilane in ethanol for 45 min, modified with 1 μM N-maleimidobutyryloxy succinimide ester (GMBS), treated with 10 μg/mL neutravidin for 30 min, and washed with 5 mL of PBS. Finally, the mixture of 10 μg/mL biotinylated EpCAM antibody (Thermo Fisher Scientific, Waltham, MA, USA), 1% (w/v) BSA, and 0.09% (w/v) sodium azide in PBS was introduced into the device for 30 min to obtain the anti-EpCAM antibody modified device. The device was stored at 4 °C, and washed with 2 mL of DEP buffer before use. All the treatments were conducted at room temperature and all the devices were modified with anti-EpCAM antibody unless specifically mentioned otherwise.

2.5. Modeling

COMSOL Multiphysics (v5.2) was used to model the electric field (AC/DC module) and the flow field (Fluid Flow module) in the main channel, and the movement of the cells in the main channel with or without the electric field (combined module of AC/DC and Fluid Flow).[32-34] All the models were solved using the Newton nonlinear method built in the software.

The governing equation for electric field simulation is $\nabla\big((\sigma + j\omega\varepsilon_0\varepsilon_r)(-\nabla V)\big) = Q_j$, and the boundary condition (excluding two side walls) is $\boldsymbol{n}\cdot\boldsymbol{J} = 0$, where σ, ω, ε_0, ε_r, V, Q_j, $\boldsymbol{n}$, and $\boldsymbol{J}$ represent conductivity (0.001 S/m), angular velocity (an alternate voltage of 200 kHz is applied), vacuum permittivity, relative permittivity (80), electric potential, charge generation (0), outward normal from the object, and current density, respectively. An alternate voltage of 12.5 V (=200/16 because 2 out of 32 columns of the microposts in the device were modeled) was applied on two side walls. The domain was discretized using triangular elements with the element sides being 1-6 μm (Fig. S1c). The DEP force experienced by a cell was calculated based on the integration of the Maxwell stress tensor on its surface, and was divided into drag and lift forces in orthogonal directions, respectively.

The governing equation for the flow field simulation is $\rho(\boldsymbol{u}\cdot\nabla)\boldsymbol{u} = -\nabla p + \mu\nabla^2\boldsymbol{u} + \boldsymbol{F}$, and the boundary condition on the sidewalls is $\boldsymbol{n}\cdot\boldsymbol{u} = 0$ (non-slip), where ρ, $\boldsymbol{u}$, p, μ, $\boldsymbol{F}$, and $\boldsymbol{n}$ represent density (1000 kg/m^3), velocity, pressure, viscosity (1 mPa.s), body force (0), and outward normal from

the object, respectively. The normal inflow speed at the inlet was 0.58 mm/s, and the pressure of the outlet was 0. The domain was discretized using triangular elements with the element sides being 1-6 μm (Fig. S1c). The flow-induced force experienced by a cell was calculated based on the integration of stress on its surface, and divided into drag and lift forces in orthogonal directions.

The governing equation for the movement of the cells with or without the electric field is $\frac{d(m_c v_c)}{dt} = \boldsymbol{F_{Flow}} + \boldsymbol{F_{DEP}}$; the flow force is $\boldsymbol{F_{Flow}} = 6\pi r_c \mu_m(\boldsymbol{u_m} - \boldsymbol{v_c})$, and the DEP force is $\boldsymbol{F_{DEP}} = 2\pi\varepsilon_m {r_c}^3 Re\left(\frac{{\varepsilon_c}^* - {\varepsilon_m}^*}{{\varepsilon_c}^* + 2{\varepsilon_m}^*}\right)\boldsymbol{\nabla}|\boldsymbol{E}|^2$ (${\varepsilon_m}^* = \varepsilon_m - \frac{j\sigma_m}{\omega}$ and ${\varepsilon_c}^* = \varepsilon_c - \frac{j\sigma_c}{\omega}$), where m_c, $\boldsymbol{v_c}$, $\boldsymbol{F_{Flow}}$, $\boldsymbol{F_{DEP}}$, r, μ, $\boldsymbol{u_m}$, $\boldsymbol{E}$, ε, σ, ω represent cell mass (cell density: 1050 kg/m^3), velocity, flow force, DEP force, radius (8 μm for cells), viscosity (1 mPa·s for medium), velocity (from flow field modeling), electric intensity, permittivity (cells: 15485 × ε_0; medium: 80 × ε_0), conductivity (cells: 0.0307 S/m; medium: 0.001 S/m), and angular velocity (an alternate voltage is applied, and frequency = 200 kHz). The subscripts *c* and *m* represent cell and medium, respectively. The electric intensity was calculated from the aforementioned electric field modeling as: $\boldsymbol{E} = -\boldsymbol{\nabla}V$. The domain was discretized using triangular elements with the element sides being 1-20 μm for numeric integration as detailed elsewhere.[32-34]

2.6. Cell culture and preparation

PC-3 human prostate cancer cells, HCT-116 human colon carcinoma cells, SK-MES-1 human lung cancer cells, OVCAR-3 human ovarian carcinoma cells, MCF-7 human breast cancer cells, and CAPAN-2 human pancreatic adenocarcinoma cells were cultured in 75 cm^2 T-flasks at 37 °C in humidified air with 5% CO_2. The medium was F12K (for PC-3 cells) and DMEM (for all other cells), supplemented with 10% fetal bovine serum (FBS), 100 U/mL penicillin, 100 μg/mL streptomycin, and 0.1% (v/v) Plasmocin^{TM} prophylactic (InvivoGen, San Diego, CA, United States). The medium was changed every two days.

To prepare WBCs for spiked cell studies, human buffy coat (Zen-Bio, Research Triangle Park, NC, United States) was lysed using red blood cell (RBC) lysis buffer to remove RBCs according to the manufacturer's instruction. The remaining cells (WBCs) were suspended at 5×10^6 WBCs /mL in DEP buffer consisting of 10% (w/v) sucrose and 0.3% (w/v) glucose in deionized water.

2.7. Scanning electron microscopy

Scanning electron microscopy **(**SEM) was used to examine the contact of captured cells with the microposts. After cell capture, cells attached on the microposts were fixed using 2.5% glutaraldehyde in phosphate buffered saline overnight. After the standard procedures of dehydration in ethanol and drying overnight, the PDMS part of the device was detached from the glass slide carefully. The cells in the main channel were sputter coated using a Cressington 108 sputter coater at 12 mA for 90 s before examination using an FEI Nova NanoSEM 400 scanning electron microscope.

2.8. Preparation of patient blood samples

Whole blood samples were obtained from nine patients with colon tumor. The protocol for obtaining the whole blood samples was approved by the Institutional Review Board (IRB) at The Ohio State University. Two healthy donors and nine patients with colon tumor were determined based on computed tomography (CT) scan of abdomen and pelvis, colonoscopy, and pathology (for patients underwent surgery already). Additional two blood samples (buffy coat) from healthy donors were purchased from Zen-Bio (Research Triangle Park, NC, USA) and used as received. The whole blood samples from patients with colon tumor were lysed using RBC lysis buffer to remove RBCs first according to the manufacturer's instruction. The remaining cells were suspended in DEP buffer of the same volume as the whole blood before RBC lysis, to obtain the final cell suspensions for further experiment. The final cell suspensions were then introduced into the integrated device for CTC capture at a flow rate of 8 mL/hr. After CTC capture, the device was treated for immunofluorescence staining of the CTCs.

2.9. Labelling of cancer cells and immunofluorescence staining of CTCs

For studies with spiked cancer cells, the cells were detached from culture flask, suspended in cell culture medium, and stained with calcein AM (0.2% (v/v)) (Life Technologies, Waltham, Massachusetts, United States) for 10 min at 37 °C. The pre-stained cells were then spiked into the aforementioned DEP buffer or WBC suspension at various cell concentrations (2-1300 cells/mL) for further experiments.

The immunofluorescence pattern of $DAPI^{+}CK20^{+}CD45^{-}$ or $DAPI^{+}CEA^{+}CD45^{-}$ was applied to

identify CTCs from WBCs. For the immunofluorescence staining of the CTCs, 4% (w/v) paraformaldehyde was introduced into the device first to fix the cells inside the device for 10 min. After fixation, 0.1% Triton X-100 in PBS was introduced into the device to permeabilize the cells for 10 min. Next, 3% (w/v) BSA in PBS was introduced into the device to block non-specific binding for 30 min. Afterward, 500 μL of FITC-labeled anti-CK20 [35,36] (abcam, ab189087, 1:50 dilution) and FITC-labeled anti-CEA [37,38] (abcam, ab106739, 1:20 dilution) in 3% (w/v) BSA solution were introduced into the device and incubated for 1 h. The device was then washed with PBS, and 500 μL of APC-labeled anti-CD45[19,39] (BD bioscience, 1:50 dilution) in 3% (w/v) BSA solution were introduced into the device and incubated for 1 h. The device was then washed with PBS, and the cells were stained with DAPI (500 nM) for 20 min to visualize the nuclei. All the treatments were conducted at room temperature unless specifically mentioned otherwise.

2.10. Monitoring temperature in microfluidic device

The temperature of the DEP buffer in the microfluidic device for CTC capture was monitored by inserting a thin thermocouple (OMEGA K series, Norwalk, CT) 5 mm into the main channel (i.e., the red region in Fig. 1a) of the device from the middle location of the open exit (Fig. S1b) of the main channel. DEP buffer was then flowed into the device at 1 mL/h, with or without applying the patterned electric voltage on the device. The microcontroller was programmed to turn the switch on (for 3 s) and off (for 1 s) in the same way as that for CTC detection studies. The temperature was recorded using an EXTECH (Nashua, NH) digital multimeter in the temperature mode.

2.11. Quantification of capture efficiency and purity

The capture efficiency was calculated as the percentage of the captured spiked cancer cells out of the total number of spiked cancer cells introduced into a device. No capture efficiency was reported for CTCs since the number or concentration in patient blood sample was unknown *a priori*. The capture purity was calculated as the percentage of the spiked cancer cells or CTCs captured in a device out of all cells (including WBCs and cancer cells/CTCs) captured in the device.

2.12. Imaging

Confocal immunofluorescence images were taken on an Olympus FluoView FV1000 confocal

microscope. All other images and movies were taken using a Zeiss Axio Observer.Z1 microscope with a Zeiss AxioCam MR3 CCD camera.

2.13. Statistical analysis

All data were reported as mean ± standard deviation from at least three independent runs. Student's two-tailed t-test assuming equal variance was analyzed using JMP Pro 13 (SAS Institute, Cary, NC) to evaluate statistical significance ($p < 0.01$).

3. Results and discussion

3.1. Design of the ZonesChip with separate capture and flow zones

The ZonesChip microfluidic device system (Fig. 1a and Figs. S1-S2) consists of two major components: (1) parallel patterned microposts modified with anti-EpCAM antibody for capturing the CTCs, and (2) electrodes placed against the inner sidewalls of the channel for generating DEP force that can move the cells and increase the cell-micropost contact frequency. More importantly, by taking advantage of the parallel design of the microposts (Fig. 1b), two different zones can be created in the main channel: (1) a capture zone (green in Fig. 1b) with low flow speed (< 0.2 mm/s, see Fig. 1c and Fig. S1c) for capturing cancer cells, and (2) a flow zone (yellow in Fig. 1b) with high flow speed (> 0.2 mm/s) (see Fig. 1c and Fig. S1c) for samples to flow through the microfluidic device. To modify the surface with anti-EpCAM, streptavidin was introduced onto the surface using the N-hydroxysuccinimide (NHS)/maleimide chemistry (Fig. S3). Prior to experiments, biotinylated anti-EpCAM was introduced into the device for antibody coating, as shown in Fig. 1a and Fig. S3.

3.2. Driving cells from the flow zone into capture zone on chip with patterned DEP

To enhance the CTC-capturing efficiency using the two zones-based ZonesChip device, DEP force was used to drive the target cells to the capture zone from the flow zone. Two electrodes are placed against the inner sidewalls of the main channel. When an electric voltage is applied on the electrodes, a heterogeneous electric field can be produced in the main channel with the electric field in the capture zone being much stronger than that in the flow zone (Fig. 1d). This may generate a DEP force on cells in the main channel, to move cells from the flow zone into the capture zone. This is because a particle such as a cell will experience a DEP force if the polarization (i.e., the complex permittivity) of the

particle is different from that of its surrounding medium. If the particle has stronger polarization, it will experience a positive DEP force towards strong electric field region; and conversely, if the particle has weaker polarization, it will experience a negative DEP force towards the weak electric field region [34]. In this study, an alternate-current (AC) electric field at a frequency of 200 kHz was applied on the device. At this frequency, the polarization of the cells (particles) is stronger than that of the surrounding DEP buffer [34]. Therefore, cells will experience a positive DEP force, and be driven from the flow zone with low electric field towards the capture zone with strong electric field (Fig. 1d). It is worth noting that DEP force that has been widely used for safe manipulation of bioparticles including living cells [26-28,34], is used as an example in this study. Nonetheless, other (e.g., acoustic) forces can also be used [40,41].

As shown in Fig. 1d, the strongest electric field is close to surface of the microposts in the capture zone. As a result, the combined force due to positive DEP and fluid flow not only can move the cells from the flow zone into the capture zone but also push the cells in the capture zone to contact with the surface of the microposts. This greatly enhances the possibility of binding between the antibody (i.e., anti-EpCAM in this study) modified on the microposts and the target cells (i.e., CTCs in this study) of the antibody, to enhance the efficiency of capturing the target cells.

When the electric field is removed, the cells that are not bound on the surface of the microposts will move back into the flow zone from the capture zone by the flow-induced force, while the targeted cells bound on the surface of the microposts may stay in the capture zones. The latter is particularly improved by the much reduced flow speed in the capture zone so that the flow-induced force is not strong enough to pull apart the binding between the target cells and the antibody modified on the surface of the microposts.

To avoid blocking of cells in the main channel with microposts, a patterned electric voltage V_{in} is applied on the electrodes by using an electric control system, as shown in Fig. S4. Fig. S4a shows the circuit for generating the patterned voltage and the real image of the electric control system consisting of a power supply, a microcontroller, and a switch. The power supply can provide a voltage of 200 V_p at the frequency of 200 kHz. As aforementioned, at this frequency, all the cells experience positive

DEP force, and are driven from weaker towards stronger electric field regions. The microcontroller can be programmed to turn the switch on/off in a controlled time pattern. In this study, it is programmed to turn the switch on (DEP is activated) for 3 s and then off (DEP is removed) for 0.25-3 s dependent on the flow rate/speed, periodically. Therefore, the voltage applied on the device is designed as shown in Fig. S4b. In a device without antibody modification, nearly all cells move in the flow zone in the absence of an electric field (i.e., switch off, Fig. 1e, left). When the switch is on, and an electric voltage (V_p = 200 V) is applied on the device (i.e., switch on), nearly all the cells are moved by the DEP force into the capture zone from the flow zone, and contact with the microposts (Fig. 1e, middle). When the switch is off again and the voltage is removed, nearly all the cells are dragged away from the capture zones and move back into the flow zones (Fig. 1e, right). These motions of the cells can be clearly seen in Movie S1 that corresponds to Fig. 1e.

These experimental observations are consistent with the modeling results on the cell movement in the main channel in the absence and presence of an electric field. As shown in Movie S2, the cells move in the flow zones and then out of the device in the absence of any electric field. When the same electric field as that for obtaining the experimental data in Fig. 1e is applied, the cells are moved into the capture zone from the flow zone and contact with the surface of the microposts (Movie S3). This indicates that the model can predict the trend of the cell movement although the effect of the cells on the flow and the interactions among the cells were not taken into consideration in this model. Therefore, the forces that the cells may experience in the flow and capture zones are further analyzed using the model to help understanding the mechanism of capturing cells on the surface of the microposts. Fig. S5 shows the DEP force experienced by a cell at four different locations in the flow zone. The direction of the DEP force is all across the flow streamlines (along which the cells would move in the absence of DEP), and towards the capture zone. This facilitates moving the cells from the flow zone into the capture zone, which is consistent with the cell movement shown in Fig. 1e and Movie S1. In addition, the drag and lift forces experienced by a static cell on the surface of a micropost were investigated. The drag force that the cell experiences is tangential to the surface of the micropost (the direction along with the local flow velocity is defined as being positive), and the lift

force is perpendicular to the surface of the micropost (outward against the micropost is defined as the positive direction). The two forces that a cell may experience in various angles (θ) on the surface of a micropost, as a result of the fluid flow and electric field (i.e., DEP), are shown in Fig. S6. The results show that the most stable positions for a cell attached on the surface of the micropost is in the capture zone with θ being less than ~30°, where the total drag force is nearly zero and the total lift force is strong towards the micropost. Moreover, the drag force increases as θ increases from 30° in the capture zone to 90° along the surface of the micropost. This may explain why cells are more likely to be captured in the capture zone and the throughput is limited if the capture and flow zones overlap.

3.3. Characterization of cell movement and capture in the ZonesChip

To understand the effect of DEP and anti-EpCAM antibody modification on cell capture using the ZonesChip, the movement of a PC-3 cell spiked into the DEP buffer was studied under different conditions (see Fig. 2). In a device with anti-EpCAM antibody modification, the cell moves straightly out of the device when no electric field is applied on the electrodes (i.e., DEP is off, Fig. 2a and Movie S4). This is because it is difficult for the cell to stably bind with the antibody coated on the micropost at the high flow speed (0.58 mm/s on average at 1 ml/hr of flow rate, which is ~4 times higher than that typically reported in the literature [17]). If a patterned electric voltage as that shown in Fig. S4b is applied on a device without antibody modification, the cell is driven from the flow zone into the capture zone to contact the microposts when the DEP is activated/on (Fig. 2b and Movie S5). When the DEP is off, the cell is washed away from the capture zone. The cell keeps moving like this repeatedly and eventually moves out of the device with the flow. With both DEP and antibody modification, the cell is driven into and stay captured in the capture zone (Fig. 2c and Movie S6). Therefore, both DEP and antibody modification are indispensable for the capture of cancer cells at the high flow speed (0.58 mm/s on average) studied here. It is worth noting that the cell shown in Fig. 2c is not captured even though it touches the microposts modified with antibody in the flow zone (θ = 90), again probably because the flow-induced drag force is very high in the flow zone with high flow speed (see Fig. S5b) to break the possible binding between the cell and microposts via the antibody.

3.4. Capture of spiked cells with the ZonesChip

To further confirm the aforementioned observations, PC-3 cells were stained with calcein AM before introducing into the device. As shown in Fig. 3a, the captured PC-3 cells are all in the capture zone, and most of them are in the middle of the capture zone. This further confirms the aforementioned force and cell movement analyses. Typical high-magnification light and scanning electron microscopy (SEM) images of a captured PC-3 cell are shown in Fig. 3a and b, respectively. These images demonstrate the surface contact between the captured cell and antibody-modified micropost, suggesting the cell is pushed against the micropost for binding with the micropost via the anti-EpCAM antibody modified on the micropost by the negative (i.e., pointing to the micropost) lift force shown in Fig. S6.

The capture efficiency of PC-3 cells spiked into the DEP buffer is further quantified under various conditions to assess the importance of separating the capture and flow zones. As shown in Fig. 3c, if there is no surface modification of the main channel with anti-EpCAM antibody, no PC-3 cells can be captured in the device regardless of DEP (conditions C: Control and D: DEP alone). If the main channel is modified with the antibody but there is no DEP (condition A: Antibody alone), the capture efficiency of PC-3 cells is still very low (1.4-0% for flow rates of 0.1-1 mL/hr). This is because in the absence of DEP, the PC-3 cells move in the flow zone and have little chance to contact the surface of the microposts in the flow zones (Fig. 2a); and even through some cells may contact the surface of the microposts in the flow zone, they may be easily washed off by the strong flow-induced drag force in the flow zone to move together with the flow, particularly at a high flow speed (e.g., 0.58 mm/s on average for the flow rate of 1 mL/hr). With both DEP and surface modification with antibody, the capture efficiency reached ~100% at all the flow rates of 0.1, 0.5, and 1 mL/hr. This is because the combined force due to DEP and fluid flow can drive the cells from the flow zone into the capture zone and push the cells towards the surface of the microposts, so that the cells are very likely to bind with antibody modified on the surface of the microposts. Once bound, the cells may stay captured because the weak flow-induced force may not be strong enough to detach the binding between the cells and the antibody modified on the microposts in the capture zone (Fig. 2c). Therefore, the capture efficiency can be increased from approximately 0 to 100% by separating the capture and flow zones, for PC-3

cells spiked in DEP buffer. Additionally, the capture efficiency of PC-3 cells spiked in DEP buffer with both DEP and antibody modification at various flow rates (0.5-4 mL/hr) is shown in Fig. 3d. At the flow rate of 1 mL/hr, the capture efficiency can reach 98.1%. As the flow rate increases from 1 to 4 mL/hr, the capture purity increases (Fig. S7), but the capture efficiency decreases. This is probably because the percentage of cells (both cancer cells and WBCs) moved into the capture zone from the flow zone by the DEP force decreases at these high flow rates due to the increased moving speed of the cells along the flow direction and the shrinkage of the capture zone with a flow speed not higher than 0.2 mm/s.

It is worth noting that the flow rate of 1 mL/hr is typically used in the literature of antibody-based CTC capture approaches [17,19]. Under this flow rate, the average flow speed in the main channel of our ZonesChip is as high as 0.58 mm/s, which is ~4 times higher than that reported in the literature for antibody-based approaches (~0.15 mm/s) [17]. A more detailed comparison of our ZonesChip (having separate capture and flow zones) and the device with overlapping capture and flow zones reported in [17] is given in Table S1. The concentration of WBCs was set as 5×10^6 or 20×10^6 cells/mL in this study while cancer cells were spiked in whole human blood in the study of [17]. The WBC concentrations used in this study are either similar to or higher than the WBC concentration (4-11 $\times$ 10^6 cells/mL, [42]) in whole human blood. As shown in Table S1, the effective capture area of our device is ~13 times smaller ($72 = 4.8 \times 15$ mm^2 in Fig. 1a versus $969 = 19 \times 51$ mm^2) than that of the device reported in [17]. In addition, the capture efficiency (91.2 ± 1.9% and 75.7 ± 10.7% for WBC concentrations of 5 and 20 $\times 10^6$ cells/mL, respectively) of our device is higher than that (~66%) of the previously reported device. When the WBC concentration is 5 $\times 10^6$ cells/mL, the capture purity of our device is higher than that reported previously (27.8 ± 8.8% versus ~9%). However, the capture purity decreases to 3.9 ± 1.5% for our device when the WBC concentration is increased to 20 $\times 10^6$ cells/mL although the capture efficiency is still higher under this condition for our device. These data suggest that the use of our ZonesChip with separate capture and flow zones could increase the throughput by ~4 times in terms of flow speed and reduce the effective capture area by 13 time without compromising the capture efficiency, compared to conventional devices with overlapping capture and

To further test the universality of the ZonesChip for capturing EpCAM+ cancer cells, six types of cancer cells with positive EpCAM expression (PC-3, HCT-116, SK-MES-1, OVCAR-3, MCF-7, and CAPAN-2 cells) spiked in WBC suspensions (5×10^6 WBCs /mL) are studied and the data are shown in Fig. 3e. The cell samples are introduced into the device at the flow rate of 1 mL/hr. For all the cancer cells, the capture efficiency can reach more than 91%, suggesting this device works efficiently for all the EpCAM+ cancer cells. The distribution of the captured PC-3 cells in the main channel is shown in Fig. S8. Nearly all the PC-3 cells were captured in the first 65 rows. This demonstrates that DEP is highly effective to drive the cells to contact the surface of the microposts in the capture zone. In addition, we investigated possible heat generation in the device by monitoring the temperature of DEP buffer inside the channel. As shown in Fig. S9, the temperature variation in the device during 30 min of experiment is negligible. This is probably because the high flow rate (1 mL/h or 0.58 mm/s in terms of the average flow speed) of the DEP buffer in the device. Given the 15 mm length of the main detection channel (Fig. 1a), the DEP buffer can flow through the detection channel in less than 30 s. The cell viability was quantified using a standard fluorescence-based live/dead assay kit. The viability was high (> 95%) for all the six types of cancer cells after capture in the device (Fig. S10). Furthermore, the captured cells can be collected (by flowing PBS through the device at 8 mL/h) and cultured in tissue culture plate with high viability (Fig. S11). These results demonstrate that the capturing procedure is not harmful to cells and it can be conducted at room temperature without the need of a heat sink to control temperature. The capture of PC-3 cells spiked at various numbers in WBC suspensions is further conducted, and the capture efficiency can be ~92% (i.e., the slope of the fitting line in Fig. 3f) on average when the spiked cell number is over a range of 2 to 1300 cells per mL (Fig. 3f). These data suggest our ZonesChip has the capacity to work effectively over a large concentration range of cancer cells in blood samples.

3.5. Capture of CTCs from patient blood samples with the ZonesChip

Finally, we tested our approach for capturing CTCs using human blood samples from patients with early or localized-stage colon tumor by using an integrated ZonesChip device. As shown in Fig. S12**,**

the integrated device consists of eight-unit devices that are connected in parallel. The unit device (Fig. 1a and Figs. S1-S2) has been tested in the aforementioned experiments using samples with spiked cancer cells. The flow rate of blood samples with the integrated device is set as 8 mL/hr, so that 1 mL of sample could be run through the device in 7.5 min (1/8 hr). The immunofluorescence pattern of $DAPI^{+}CK20^{+}CD45^{-}$ or $DAPI^{+}CEA^{+}CD45^{-}$ is used to identify CTCs from WBCs in the main channel of the integrated device. As shown in Fig. 4a, the CTCs are lit up by green fluorescence ($CK20^{+}/CEA^{+}$) while the WBCs are visualized by red fluorescence ($CD45^{+}$). CTCs in blood samples of 9 patients with colon tumor (CT1-CT9) are detected and the results are shown in Fig. 4b and Table S2. CTCs (32-424) can be detected in 1 mL of blood from all the 9 patients with colon tumor, which indicates that the device is capable of working over a large range of CTC concentration in blood. The purity of CTC capture with our device is 28.3±7.6%. This capture purity with cancer patient samples where the WBC concentration is the same as that in whole human blood, is close to the ~27.8% capture purity for the spiked cancer cells in DEP buffer with the WBC concentration of 5×10^{6} cells/mL shown in Table S1. This suggests the condition with 5×10^{6} WBCs/mL might better mimic whole human blood than the condition with 20×10^{6} WBCs/mL for the studies with spiked cancer cells. In addition, it supports the aforementioned claim that our ZonesChip could be used to enhance the throughput of microfluidic detection of CTCs without compromising the capture efficiency (and possibly capture purity), compared to conventional devices with overlapping capture and flow zones.

This is comparable to that (~10-50%) reported in the literature for antibody-based microfluidic approaches and much better than the immunomagnetic-bead purification approach (~0.01% in purity) that is the leading technology currently used in the clinic [17,18,22]. It may be possible to achieve higher purity by using antibodies that are more specific to CTCs and by increasing the flow rate to wash away WBCs that are more weakly attached to the microposts than CTCs (Fig. S7). However, the latter could also result in a decrease of the capture efficiency (Fig. 3d). Due to the rarity of CTCs in blood (especially for early stage cancer), a high capture efficiency is of the utmost importance and a slight sacrifice of purity may be acceptable. In addition to single CTCs, we also observed few cell clusters of CTCs and WBCs in 5 out of 9 patients (Fig. S13), which is consistent with a work reported

recently [43]. Blood samples from four healthy donors (HD1-HD4) were tested using this device, and no CTCs were captured from these blood samples. Our data using blood samples from both cancerous and healthy patients demonstrate the great potential of our approach for practical CTC detection.

4. Conclusions

In summary, we developed an antibody-based microfluidic approach for CTC detection with separate capture and flow zones to greatly enhance the throughput with high detection efficiency. This is achieved by minimizing the flow speed and thus flow-induced force in the capture zone even at flow speeds that are ~4 times higher than that commonly used in the literature, and by using DEP force to move cells from the flow zone into the capture zone. Moreover, this approach requires a much smaller effective capture area for CTC detection. Although this work is focused on CTC detection from human blood, the idea of separating the flow zone from the capture zone may be applicable to enhance the detection or isolation of any rare cells or particles including exosomes and macromolecules using microfluidics. Besides the DEP force used as the example in this study, other (e.g. acoustic) forces can also be utilized to move particles from the flow zone into the capture zone to facilitate the contact between the particles and the antibody (or other agents)-modified surface in the capture zone. Therefore, this idea of separating the flow zone from the capture zone has an immense potential to enhance microfluidics-based disease detection.

Acknowledgments

This work was partially supported by grants from American Cancer Society (ACS #120936-RSG-11-109-01-CDD) and NIH (R01CA206366) to X.H., and a Pelotonia post-doctoral Fellowship to J.X. We would like express our special thanks to Mr. Andrew Suzo and Ms. Kayla Diaz for their help with the procurement of patient blood samples.

Appendix A. Supplementary data

Supplementary data related to this article can be found at http://

Data availability

All data supporting the findings of this study are available from the corresponding authors upon request.

REFERENCES

[1] S.R. L., M.K. D., J. Ahmedin, Cancer statistics, 2018, CA Cancer J Clin 68(1) (2018) 7-30.

[2] R.L. Siegel, K.D. Miller, A. Jemal, Cancer statistics, 2018, CA Cancer J Clin 68(1) (2018) 7-30.

[3] S. Rebecca, D. Carol, J. Ahmedin, Colorectal cancer statistics, 2014, CA Cancer J Clin 64(2) (2014) 104-117.

[4] T. Kitamura, B.-Z. Qian, J.W. Pollard, Immune cell promotion of metastasis, Nature Reviews Immunology 15 (2015) 73.

[5] J. Massagué, A.C. Obenauf, Metastatic colonization by circulating tumour cells, Nature 529 (2016) 298.

[6] M. Cristofanilli, G.T. Budd, M.J. Ellis, A. Stopeck, J. Matera, M.C. Miller, J.M. Reuben, G.V. Doyle, W.J. Allard, L.W. Terstappen, Circulating tumor cells, disease progression, and survival in metastatic breast cancer, New England Journal of Medicine 351(8) (2004) 781-791.

[7] V. Plaks, C.D. Koopman, Z. Werb, Circulating tumor cells, Science 341(6151) (2013) 1186-1188.

[8] J.S. De Bono, H.I. Scher, R.B. Montgomery, C. Parker, M.C. Miller, H. Tissing, G.V. Doyle, L.W. Terstappen, K.J. Pienta, D. Raghavan, Circulating tumor cells predict survival benefit from treatment in metastatic castration-resistant prostate cancer, Clinical cancer research 14(19) (2008) 6302-6309.

[9] M. Kalinich, I. Bhan, T.T. Kwan, D.T. Miyamoto, S. Javaid, J.A. LiCausi, J.D. Milner, X. Hong, L. Goyal, S. Sil, M. Choz, U. Ho, R. Kapur, A. Muzikansky, H.D. Zhang, D.A. Weitz, L.V. Sequist, D.P. Ryan, R.T. Chung, A.X. Zhu, K.J. Isselbacher, D.T. Ting, M. Toner, S. Maheswaran, D.A. Haber, An RNA-based signature enables high specificity detection of circulating tumor cells in hepatocellular carcinoma, Proc Natl Acad Sci U S A 114(5) (2017) 1123-1128.

[10] L.S. Sasportas, S.S. Hori, G. Pratx, S.S. Gambhir, Detection and Quantitation of Circulating Tumor Cell Dynamics by Bioluminescence Imaging in an Orthotopic Mammary Carcinoma Model, PLoS One 9(9) (2014).

[11] S. Rawal, Y.P. Yang, R. Cote, A. Agarwal, Identification and Quantitation of Circulating Tumor Cells, Annu Rev Anal Chem 10 (2017) 321-343.

[12] G. Simone, G. Perozziello, E. Battista, F. De Angelis, P. Candeloro, F. Gentile, N. Malara, A. Manz, E. Carbone, P. Netti, E. Di Fabrizio, Cell rolling and adhesion on surfaces in shear flow. A model for an antibody-based microfluidic screening system, Microelectronic Engineering 98 (2012) 668-671.

[13] G. Simone, N. Malara, V. Trunzo, G. Perozziello, P. Neuzil, M. Francardi, L. Roveda, M. Renne, U. Prati, V. Mollace, A. Manz, E. Di Fabrizio, Protein–Carbohydrate Complex Reveals Circulating Metastatic Cells in a Microfluidic Assay, Small 9(12) (2013) 2152-2161.

[14] G. Simone, P. Neuzil, G. Perozziello, M. Francardi, N. Malara, E. Di Fabrizio, A. Manz, A facile in situ microfluidic method for creating multivalent surfaces: toward functional glycomics, Lab Chip 12(8) (2012) 1500-1507.

[15] K.H.K. Wong, S.N. Tessier, D.T. Miyamoto, K.L. Miller, L.D. Bookstaver, T.R. Carey, C.J. Stannard, V. Thapar, E.C. Tai, K.D. Vo, E.S. Emmons, H.M. Pleskow, R.D. Sandlin, L.V. Sequist, D.T. Ting, D.A. Haber, S. Maheswaran, S.L. Stott, M. Toner, Whole blood stabilization for the microfluidic isolation and molecular characterization of circulating tumor cells, Nat Commun 8(1) (2017) 1733.

[16] M.-H. Park, E. Reátegui, W. Li, S.N. Tessier, K.H.K. Wong, A.E. Jensen, V. Thapar, D. Ting, M. Toner, S.L. Stott, P.T. Hammond, Enhanced Isolation and Release of Circulating Tumor Cells Using Nanoparticle Binding and Ligand Exchange in a Microfluidic Chip, Journal of the American Chemical Society 139(7) (2017) 2741-2749.

[17] S. Nagrath, L.V. Sequist, S. Maheswaran, D.W. Bell, D. Irimia, L. Ulkus, M.R. Smith, E.L. Kwak, S. Digumarthy, A. Muzikansky, P. Ryan, U.J. Balis, R.G. Tompkins, D.A. Haber, M. Toner, Isolation of rare circulating tumour cells in cancer patients by microchip technology, Nature 450(7173) (2007) 1235-9.

[18] S.L. Stott, C.H. Hsu, D.I. Tsukrov, M. Yu, D.T. Miyamoto, B.A. Waltman, S.M. Rothenberg, A.M. Shah, M.E. Smas, G.K. Korir, F.P. Floyd, A.J. Gilman, J.B. Lord, D. Winokur, S. Springer, D. Irimia, S. Nagrath, L.V. Sequist, R.J. Lee, K.J. Isselbacher, S. Maheswaran, D.A. Haber, M.

Toner, Isolation of circulating tumor cells using a microvortex-generating herringbone-chip, Proc Natl Acad Sci U S A 107(43) (2010) 18392-18397.
[19] H.J. Yoon, T.H. Kim, Z. Zhang, E. Azizi, T.M. Pham, C. Paoletti, J. Lin, N. Ramnath, M.S. Wicha, D.F. Hayes, Sensitive capture of circulating tumour cells by functionalized graphene oxide nanosheets, Nat Nanotechnol 8(10) (2013) 735-741.
[20] W.A. Sheng, O.O. Ogunwobi, T. Chen, J.L. Zhang, T.J. George, C. Liu, Z.H. Fan, Capture, release and culture of circulating tumor cells from pancreatic cancer patients using an enhanced mixing chip, Lab Chip 14(1) (2014) 89-98.
[21] J.H. Myung, M.J. Eblan, J.M. Caster, S. Park, M.J. Poellmann, K. Wang, J.E. Tepper, K.A. Tam, S.M. Miller, C. Shen, R.C. Chen, T. Zhang, B. Chera, A.Z. Wang, S. Hong, Multivalent binding and biomimetic cell rolling improves the sensitivity and specificity of circulating tumor cell capture, Clin Cancer Res (2018).
[22] P. Li, Z.M. Mao, Z.L. Peng, L.L. Zhou, Y.C. Chen, P.H. Huang, C.I. Truica, J.J. Drabick, W.S. El-Deiry, M. Dao, S. Suresh, T.J. Huang, Acoustic separation of circulating tumor cells, Proc Natl Acad Sci U S A 112(16) (2015) 4970-4975.
[23] M. Dhar, E. Pao, C. Renier, D.E. Go, J. Che, R. Montoya, R. Conrad, M. Matsumoto, K. Heirich, M. Triboulet, J.Y. Rao, S.S. Jeffrey, E.B. Garon, J. Goldman, N.P. Rao, R. Kulkarni, E. Sollier-Christen, D. Di Carlo, Label-free enumeration, collection and downstream cytological and cytogenetic analysis of circulating tumor cells, Scientific Reports 6 (2016).
[24] J. Che, V. Yu, E.B. Garon, J.W. Goldman, D. Di Carlo, Biophysical isolation and identification of circulating tumor cells, Lab Chip 17(8) (2017) 1452-1461.
[25] X. Qin, S. Park, S.P. Duffy, K. Matthews, R.R. Ang, T. Todenhofer, H. Abdi, A. Azad, J. Bazov, K.N. Chi, P.C. Black, H.S. Ma, Size and deformability based separation of circulating tumor cells from castrate resistant prostate cancer patients using resettable cell traps, Lab Chip 15(10) (2015) 2278-2286.
[26] V. Gupta, I. Jafferji, M. Garza, V.O. Melnikova, D.K. Hasegawa, R. Pethig, D.W. Davis, ApoStream (TM), a new dielectrophoretic device for antibody independent isolation and recovery of viable cancer cells from blood, Biomicrofluidics 6(2) (2012).
[27] H.S. Moon, K. Kwon, S.I. Kim, H. Han, J. Sohn, S. Lee, H.I. Jung, Continuous separation of breast cancer cells from blood samples using multi-orifice flow fractionation (MOFF) and dielectrophoresis (DEP), Lab Chip 11(6) (2011) 1118-1125.
[28] S. Shim, K. Stemke-Hale, A.M. Tsimberidou, J. Noshari, T.E. Anderson, P.R.C. Gascoyne, Antibody-independent isolation of circulating tumor cells by continuous-flow dielectrophoresis, Biomicrofluidics 7(1) (2013).
[29] M.E. Warkiani, G. Guan, K.B. Luan, W.C. Lee, A.A. Bhagat, P.K. Chaudhuri, D.S. Tan, W.T. Lim, S.C. Lee, P.C. Chen, C.T. Lim, J. Han, Slanted spiral microfluidics for the ultra-fast, label-free isolation of circulating tumor cells, Lab Chip 14(1) (2014) 128-37.
[30] W. Chen, S. Weng, F. Zhang, S. Allen, X. Li, L. Bao, R.H. Lam, J.A. Macoska, S.D. Merajver, J. Fu, Nanoroughened surfaces for efficient capture of circulating tumor cells without using capture antibodies, ACS Nano 7(1) (2013) 566-75.
[31] A. Salmanzadeh, M.B. Sano, H. Shafiee, M.A. Stremler, R.V. Davalos, Isolation of rare cancer cells from blood cells using dielectrophoresis, Conf Proc IEEE Eng Med Biol Soc 2012 (2012) 590-3.
[32] M. Sun, P. Durkin, J. Li, T.L. Toth, X. He, Label-Free On-Chip Selective Extraction of Cell-Aggregate-Laden Microcapsules from Oil into Aqueous Solution with Optical Sensor and Dielectrophoresis, ACS Sens 3(2) (2018) 410-417.
[33] H. Huang, M. Sun, T. Heisler-Taylor, A. Kiourti, J. Volakis, G. Lafyatis, X. He, Stiffness-Independent Highly Efficient On-Chip Extraction of Cell-Laden Hydrogel Microcapsules from Oil Emulsion into Aqueous Solution by Dielectrophoresis, Small 11(40) (2015) 5369-74.
[34] M. Sun, P. Agarwal, S. Zhao, Y. Zhao, X. Lu, X. He, Continuous On-Chip Cell Separation Based on Conductivity-Induced Dielectrophoresis with 3D Self-Assembled Ionic Liquid Electrodes, Anal Chem 88(16) (2016) 8264-8271.
[35] S. Wildi, J. Kleeff, H. Maruyama, C.A. Maurer, H. Friess, M.W. Büchler, A.D. Lander, M. Korc,

Characterization of Cytokeratin 20 Expression in Pancreatic and Colorectal Cancer, Clinical Cancer Research 5(10) (1999) 2840-2847.
[36] P. Bu, K.-Y. Chen, Joyce H. Chen, L. Wang, J. Walters, Yong J. Shin, Julian P. Goerger, J. Sun, M. Witherspoon, N. Rakhilin, J. Li, H. Yang, J. Milsom, S. Lee, W. Zipfel, Moonsoo M. Jin, Zeynep H. Gümüş, Steven M. Lipkin, X. Shen, A microRNA miR-34a-Regulated Bimodal Switch Targets Notch in Colon Cancer Stem Cells, Cell Stem Cell 12(5) (2013) 602-615.
[37] J. Tiernan, S. Perry, E. Verghese, N. West, S. Yeluri, D. Jayne, T. Hughes, Carcinoembryonic antigen is the preferred biomarker for in vivo colorectal cancer targeting, British journal of cancer 108(3) (2013) 662.
[38] C.A. Metildi, S. Kaushal, G.A. Luiken, M.A. Talamini, R.M. Hoffman, M. Bouvet, Fluorescently labeled chimeric anti-CEA antibody improves detection and resection of human colon cancer in a patient-derived orthotopic xenograft (PDOX) nude mouse model, J Surg Oncol 109(5) (2014) 451-458.
[39] M. Takakura, S. Kyo, M. Nakamura, Y. Maida, Y. Mizumoto, Y. Bono, X. Zhang, Y. Hashimoto, Y. Urata, T. Fujiwara, M. Inoue, Circulating tumour cells detected by a novel adenovirus-mediated system may be a potent therapeutic marker in gynaecological cancers, British journal of cancer 107 (2012) 448.
[40] M. Wu, P.-H. Huang, R. Zhang, Z. Mao, C. Chen, G. Kemeny, P. Li, A.V. Lee, R. Gyanchandani, A.J. Armstrong, M. Dao, S. Suresh, T.J. Huang, Circulating Tumor Cell Phenotyping via High-Throughput Acoustic Separation, Small 14(32) (2018) 1801131.
[41] Y. Chen, M. Wu, L. Ren, J. Liu, P.H. Whitley, L. Wang, T.J. Huang, High-throughput acoustic separation of platelets from whole blood, Lab Chip 16(18) (2016) 3466-3472.
[42] J.G. Hollowell, O.W. van Assendelft, E.W. Gunter, B.G. Lewis, M. Najjar, C. Pfeiffer, C. Centers for Disease, N.C.f.H.S. Prevention, Hematological and iron-related analytes--reference data for persons aged 1 year and over: United States, 1988-94, Vital Health Stat 11 (247) (2005) 1-156.
[43] X. Jiang, K.H.K. Wong, A.H. Khankhel, M. Zeinali, E. Reategui, M.J. Phillips, X. Luo, N. Aceto, F. Fachin, A.N. Hoang, W. Kim, A.E. Jensen, L.V. Sequist, S. Maheswaran, D.A. Haber, S.L. Stott, M. Toner, Microfluidic isolation of platelet-covered circulating tumor cells, Lab Chip 17(20) (2017) 3498-3503.

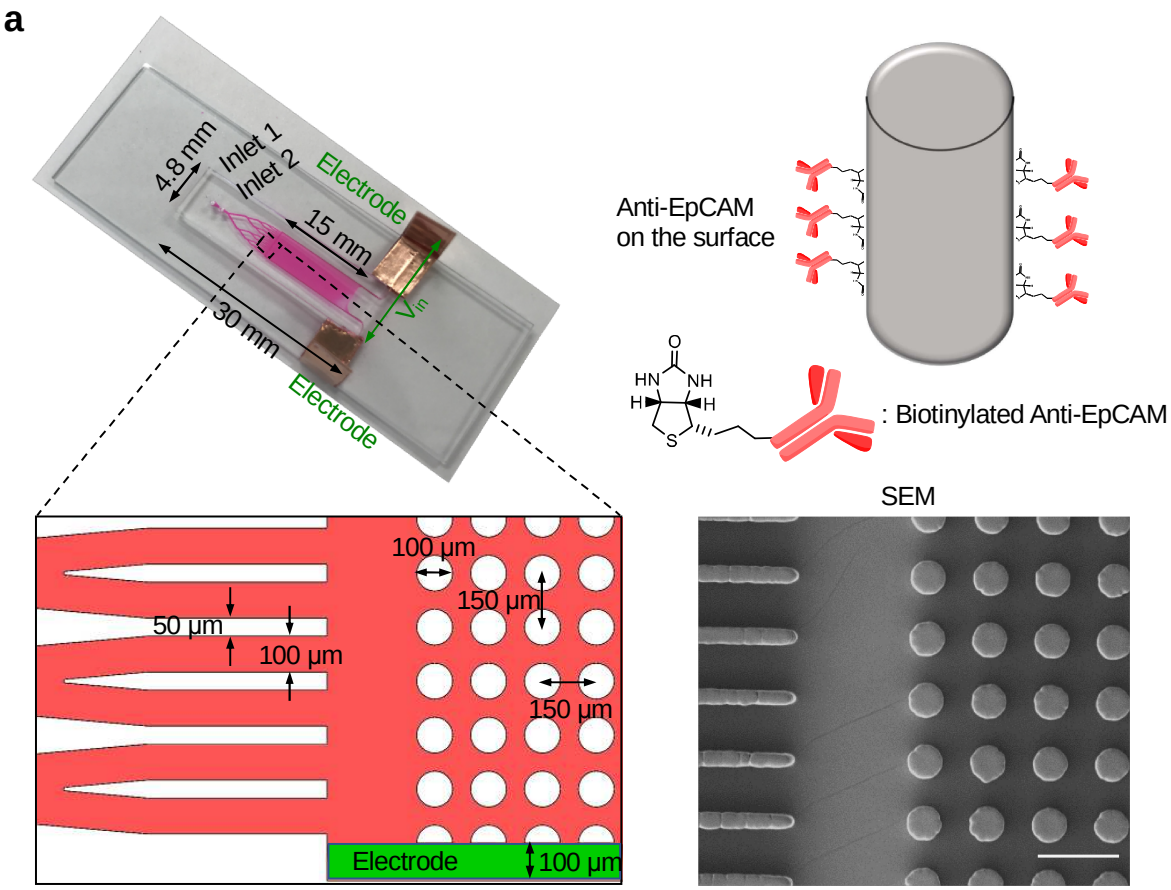
a
4.8 mm
Inlet 1
Inlet 2
Electrode
15 mm
30 mm
Electrode
Anti-EpCAM
on the surface
: Biotinylated Anti-EpCAM
100 μm
150 μm
50 μm
100 μm
150 μm
Electrode
100 μm
SEM

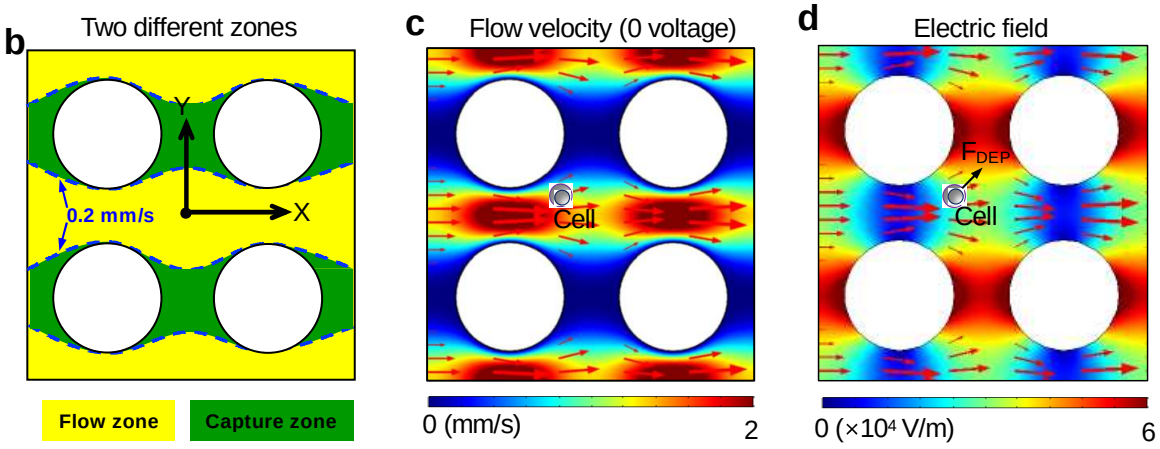
b
Two different zones
Y
X
0.2 mm/s
Flow zone
Capture zone
c
Flow velocity (0 voltage)
Cell
0 (mm/s)
2
d
Electric field
FDEP
Cell
0 (×10⁴ V/m)
6


Overall flow direction

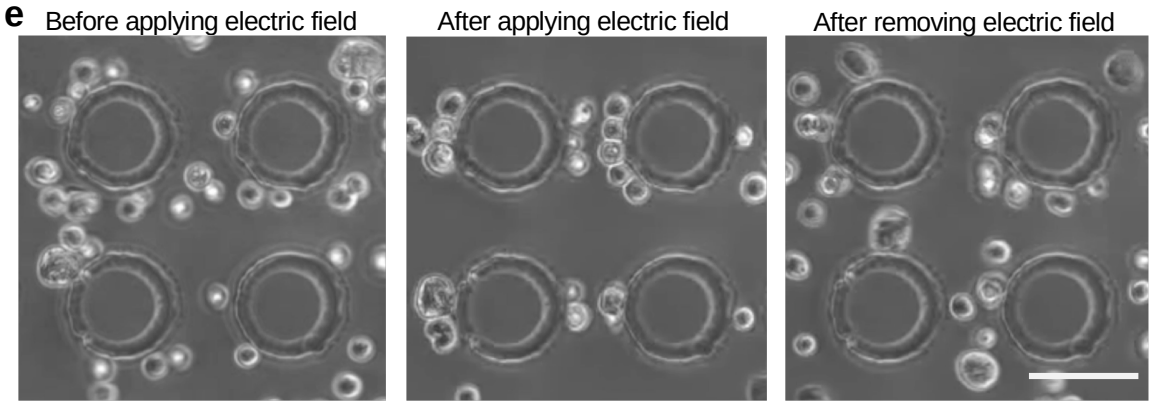
e
Before applying electric field
After applying electric field
After removing electric field

Figure 1. Characterization of the microfluidic device with separate capture and flow zones (ZonesChip). (**a**) A real image of the microfluidic device on a glass slide together with a scheme showing the chemistry of anti-EpCAM modification on the micropost in the device, and a sketch and scanning electron microscopy (SEM) image showing the placement and design of the electrodes (green) and microposts (100 rows and 32 columns in the horizontal and vertical directions, respectively) in the main channel of the device. Scale bar: 200 µm. (**b**) A schematic illustration of the capture (green) versus flow (yellow) zones in the main channel of the microfluidic device. The flow speed within the capture zone is no more than 0.2 mm/s. The overall flow direction is from left to right. (**c**) The flow speed distribution in the capture and flow zones from modeling study. The red arrows indicate the local direction of fluid flow. The flow speed is high (> 0.2 mm/s) in the flow zone while it is low (< 0.2 mm/s) in the capture zone. This can reduce the possibility of washing off cells captured in the capture zone when the overall flow rate is high. In the absence of an additional force, cells are driven by the flow-induced force to move together with the surrounding fluid in the flow zone with little chance to touch the microposts. (**d**) The electric field distribution in the capture and the flow zones from modeling with V_{in} being 12.5 V on two columns of the posts (i.e., equivalent to 200 V on 32 columns in total). The red arrows indicate the local direction of flow. The positive DEP force can drive cells from the weak electric field region towards strong electric field region. As a result, the DEP force (F_{DEP}) can help to drive cells from the flow zone into the capture zone. (**e**) The position of cells before DEP is on (i.e., switch off, left), after DEP is on (switch on, middle), and after DEP is removed (i.e., switch off, right) in a microfluidic device without surface modification. Before the switch is on, nearly all the cells are in the flow zone. After the switch is on, nearly all the cells are moved from the flow zone into the capture zone. When the switch is off again, nearly all the cells are moved back from the capture zone into the flow zone. The flow rate is 1 mL/hr for all the modeling and experimental studies. Scale bar: 100 µm.

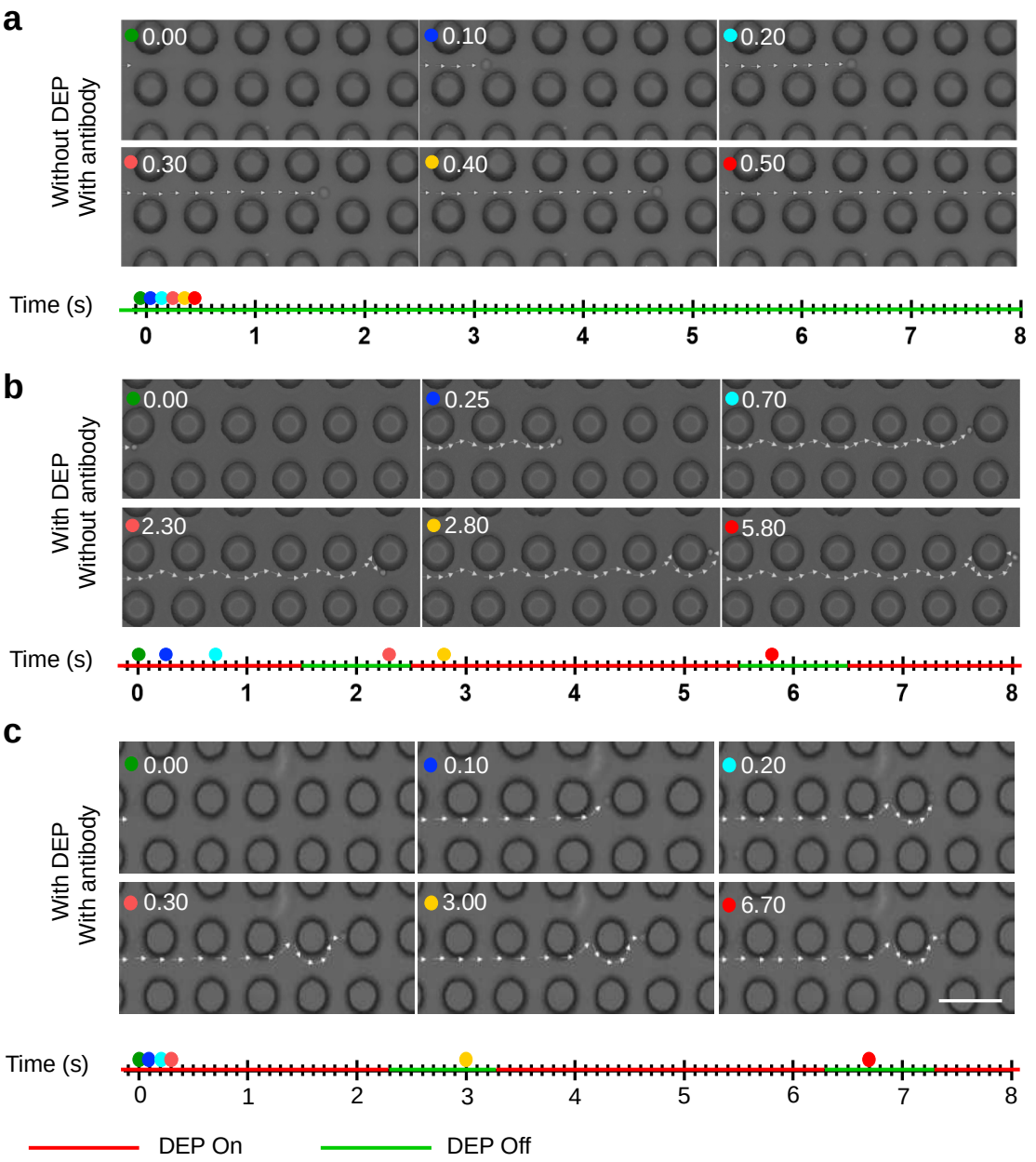

Figure 2. Characterization of the movement of a cell in the main channel of the ZonesChip under different conditions. (**a**) With surface modification of antibody but no DEP. The cell moved straightly out of the device in approximately 0.5 s. (**b**) With patterned DEP but no surface modification. The cell is driven by the positive DEP force from the flow zone into the capture zone and contacted the surface of the micropost in the middle of the capture zone when the DEP is on. When the DEP is off, the cell is washed away from the middle of the capture zone, kept moving like this repeatedly, and eventually washed out of the device by the flow. (**c**) With both surface modification and patterned DEP. The cell is driven from the flow zone to the capture zone, captured on the surface of the micropost in the middle of the capture zone at ~0.3 s, and stay there thereafter. The white arrows show the trace of the cell movement in the device. The flow rate is 1 mL/hr with an equivalent flow speed of 0.58 mm/s. The data suggest the importance of separating the flow and capture zones for sensitive capture of CTCs. Scale bar: 200 µm.

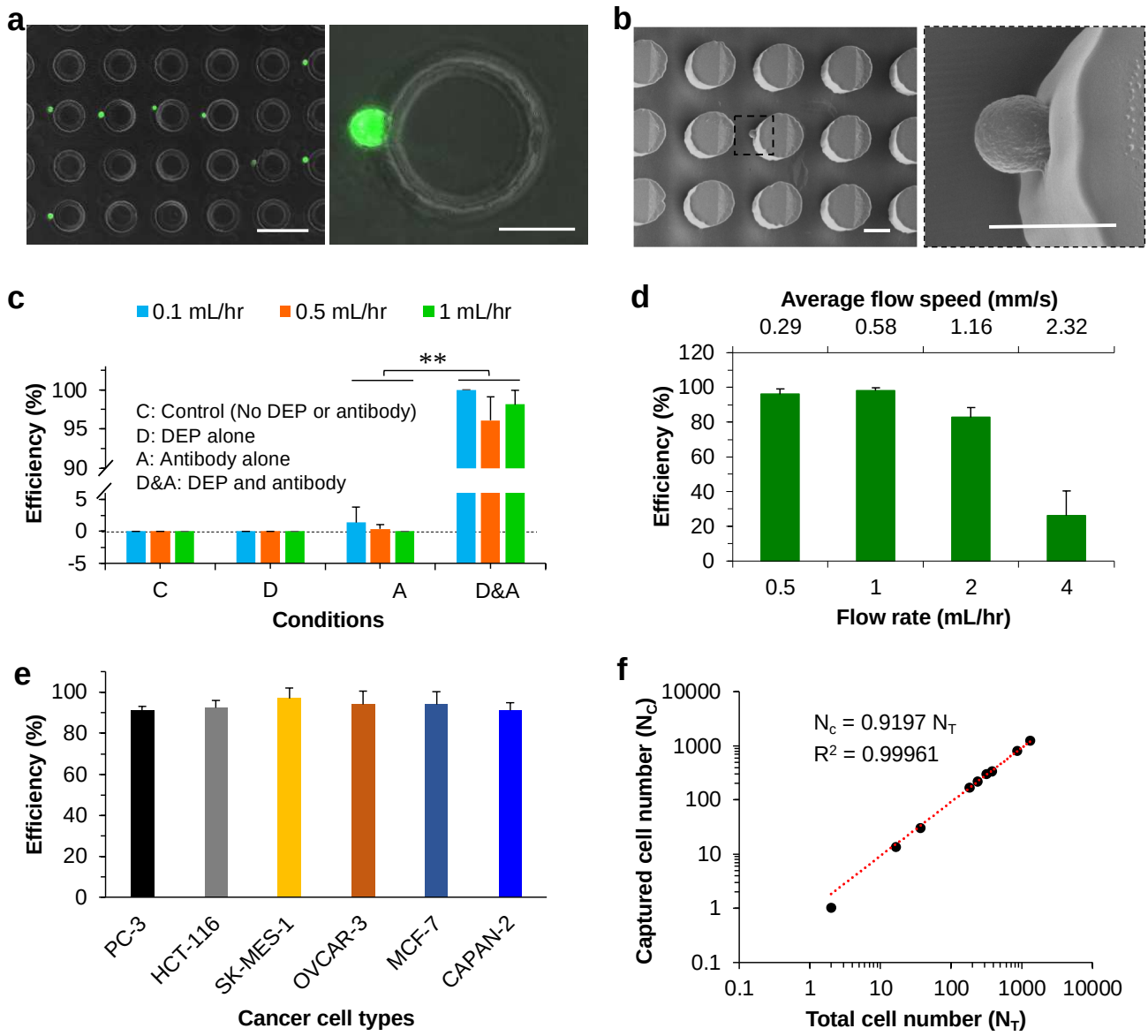

Figure 3. Characterization of the capture of cancer cells spiked in medium using the ZonesChip. (**a**) Merged view of bright field and fluorescence microscopy images showing the capture of PC-3 cells on the surface of the microposts. Most of the cells are captured in the middle of the capture zones. The PC-3 cells are labeled with calcein AM (a green fluorescent probe that has been used for staining viable cells) for visualization. Scale bar: 150 µm. The zoom-in merged view of bright field and fluorescence microscopy images shows the surface contact between the PC-3 cell and micropost. Scale bar: 50 µm. (**b**) SEM image showing the surface contact between the PC-3 cell and micropost. Scale bar: 50 µm. The cell number is reduced compared to the fluorescence image, probably due to the loss of cells during the SEM sample preparation. (**c**) The enhancement of capture efficiency by separating the capture and flow zones. With both DEP and antibody surface modification, the capture efficiency is ~100% at all three flow rates while it is nearly zero (less than 1.4%) for the device with antibody surface modification in the absence of DEP. For the latter, there is no separation of the flow and capture zones because cells dominantly stay in the flow zone in the main channel. The PC-3 cells are spiked in the DEP medium at ~500 cells per mL. (**d**) The capture efficiency at various flow rates (or various average flow speed in the main channel). The capture efficiency can reach more than 98% when the flow rate is 1 mL/hr with an equivalent flow speed that is ~8 times higher than that commonly used in the literature. The PC-3 cells are suspended in the DEP medium at ~500 cells per mL. (**e**) The capture efficiency for six different types of cancer cells spiked in white blood cell (WBC) suspension (~5×10^6 WBCs/mL). The flow rate is 1 mL/hr. For all the six types of cells, the capture efficiency can reach more than 90%. (**f**) The capture efficiency at various numbers of PC-3 cells spiked in WBC suspension (~5×10^6 WBCs/mL). The flow rate is 1 mL/hr. The capture efficiency can

be ~92% on average when the density of spiked PC-3 cells are over the range of 2-1300 cells/mL. All error bars represent standard deviation (n = 3). **: $p < 0.01$

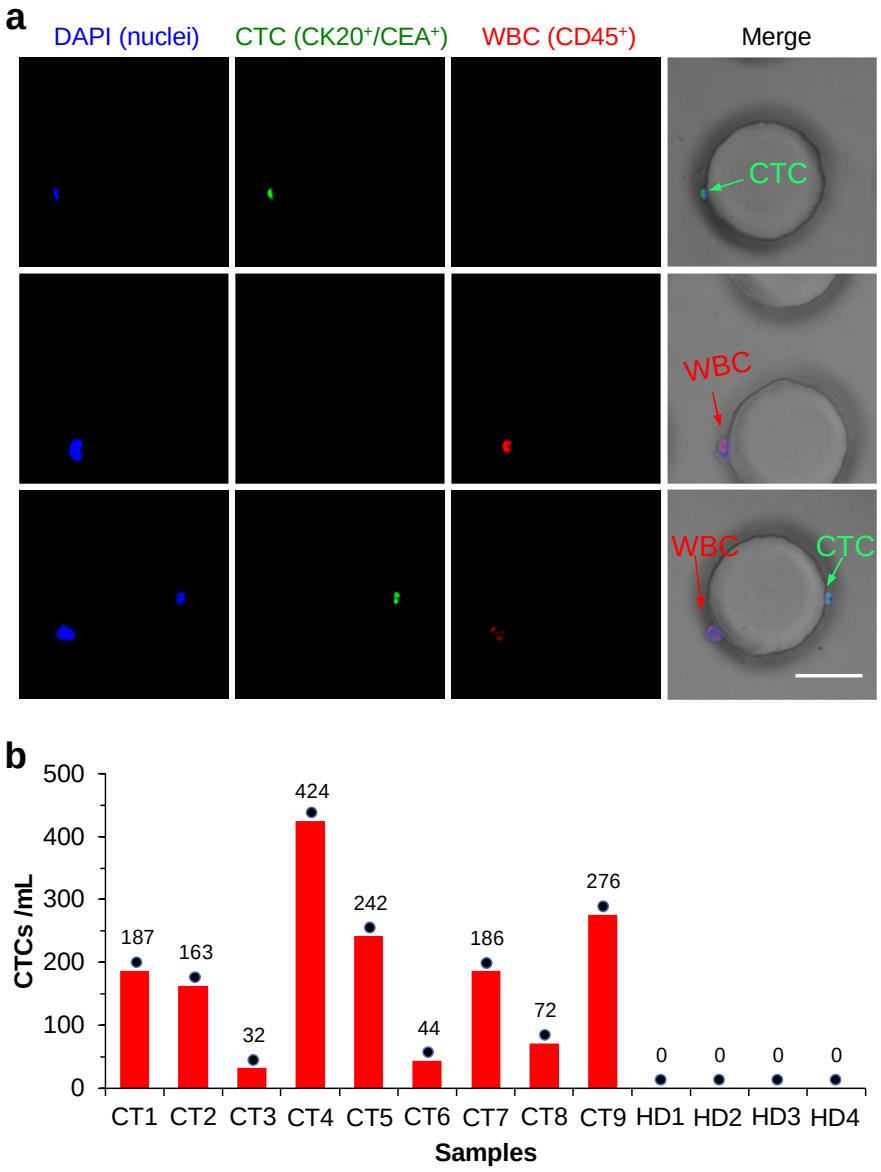

Figure 4. Detection of CTCs in blood from patients with early/localized colon tumor and healthy donors using an integrated device of the ZonesChip. (**a**) Immunofluorescence and merged (with bright field) images showing the captured CTCs on the surface of microposts. The CTCs are identified by the green fluorescence of CK20/CEA antibody, and the WBCs were identified with the red fluorescence of CD45 antibody. Scale bar: 50 µm. (**b**) The numbers of captured CTCs from blood samples of nine (CT1-CT9) patients with colon tumor and four healthy donors (HD1-HD4). The number of captured CTCs from patient blood samples varies from 32-424 cells per mL and no CTC can be captured from the blood of healthy donors.